

Enhancement in the photocatalytic activity of Ag loaded N-doped TiO₂ nanocomposite under sunlight

R. S. Dhabbe · A. N. Kadam · M. B. Suwarnkar ·
M. R. Kokate · K. M. Garadkar

Received: 22 March 2014 / Accepted: 9 May 2014 / Published online: 21 May 2014
© Springer Science+Business Media New York 2014

Abstract A N-doped titania–silver nanocomposites have been prepared by simple microwave assisted and impregnation–reduction method for the first time. As synthesized nanocomposites with different Ag contents were characterized for their phase purity, morphology, particle size, optical properties and elemental composition. It is found that N-doped TiO₂ silver nanocomposites are pure in anatase phase with an average crystallite size of 10 nm. The catalyst was tested for dye degradation and photodegradation efficiency was found to be 99.6 and 88.7 % within 90 min under UV and sunlight respectively. A 40 % enhancement in the photodegradation efficiency was achieved by Ag loading in comparison with the N-TiO₂ under sunlight. The fluorescence quenching of Ag loaded N-TiO₂ indicates decrease in rate of electron–hole pair recombination that enhances photocatalytic performance. The effects of photocatalytic operational parameters such as method of surface modification, catalyst loading and irradiation sources on the photodegradation of methyl orange were also investigated.

1 Introduction

Nanocrystalline TiO₂ photocatalyst has attracted significant attention in environmental remediation and energy generation [1–4], owing to its unique chemical and physical properties such as high catalytic activity, chemically stable, easy availability, nontoxic and low cost [5, 6]. Due to these

advantages TiO₂ has been widely investigated for the photocatalytic degradation of hazardous organic contaminants from wastewater [7, 8]. However, TiO₂ has a wide band gap (3.20 eV) that makes it active only in the UV region [9]. Also rapid recombination of photogenerated electron–hole pairs takes place which often results in low degradation efficiency. These above mentioned obstacles limit its practical applications. Therefore several doping strategies have been used to tune the band gap of TiO₂ into the visible region. Recent reports on the use of various dopants such as nitrogen, sulfur, carbon [10] and noble metals like Ag, Au, Pt, Pd [11, 12] have produced both positive and negative effects. For example, titania doped with inorganic or metallic species such as metal ions or clusters exhibited reasonably efficiently data but the structure of TiO₂ becomes unstable [13]. Notably TiO₂ doped with transition metals does not show desirable photocatalytic efficiencies due to their fast recombination rate [14]. Therefore, considerable efforts have been addressed to develop a photocatalyst active over large region of solar spectrum which can restrain the recombination of electron–hole pairs. The doping of nitrogen helps to enhance the visible light absorption capacity by narrowing the band gap of TiO₂, even though the rate of recombination of electron–hole pairs is higher. In order to overcome this difficulty, modification of N-doped TiO₂ was achieved by using noble metal nanoparticles. The noble metal nanoparticles can effectively enhance the charge carrier separation by forming a Schottky barrier on the surface of TiO₂. Generation of surface plasmon resonance could help to shift the absorption of the TiO₂ in the visible region [15–17]. There are several methods available for metal doping such as chemical reduction, ion impregnation, impregnation–reduction and photodeposition [18–20]. Particularly in photoreduction method the metal

R. S. Dhabbe · A. N. Kadam · M. B. Suwarnkar ·
M. R. Kokate · K. M. Garadkar (✉)
Nanomaterials Research Laboratory, Department of Chemistry,
Shivaji University, Kolhapur 416004, MS, India
e-mail: kmg_chem@unishivaji.ac.in

cannot be dispersed uniformly on the surface of TiO₂ [21]. To overcome this difficulty the impregnation–reduction method was employed for uniform distribution of Ag on surface of TiO₂. In this method, adsorption of metal ions takes place on the surface TiO₂ followed by reduction of Ag with NaBH₄ produced higher dispersed state of metal [22]. There are many reports on Ag doping of metal oxides [23, 24] because it has a relatively high work function which can generate surface plasmon resonance and acts as an antenna to trap electrons thereby enhancing charge transfer processes [25]. In the past decade, many researchers have investigated the surface modification of commercially available Degussa P25 (TiO₂) by metal loading. To date there are only few papers reported on Ag loaded N-doped TiO₂ photocatalyst [26, 27]. There is a need to develop a cost effective and ecofriendly methodology to synthesize nanocomposites that show high photocatalytic performance under natural sunlight.

To the best of our knowledge, we report here for the first time the preparation of Ag loaded N-doped TiO₂ nanocomposites by using simple combination of microwave followed by impregnation–reduction method. This preparation route offers the tuning of the band gap of TiO₂ to a desired level through loading of Ag nanoparticles. The Ag loaded N-doped TiO₂ nanocomposites were then characterized and tested for degradation of methyl orange (MO) under UV and sunlight. In the case of simple impregnation method, leaching of Ag nanoparticles was observed which as confirmed by the shifting of MO peak during the photodegradation whereas the impregnation–reduction method was significantly more effective in terms of photocatalytic activity.

2 Experimental

2.1 Materials

Titanium tetra-isopropoxide (TTIP, 98 %), cetyl trimethyl ammonium bromide (CTAB, 99 %) were purchased from Spectrochem Pvt. Ltd., Mumbai (India). 25 % ammonia was purchased from Loba Chemie Pvt. Ltd., Mumbai (India). Silver nitrate was purchased from Merck, Mumbai. Absolute ethanol (99.9 %) was purchased from Changshu Yangquan Chemicals, China and sodium dodecyl sulfate (SDS, extrapure) was purchased from Thomas Baker Pvt. Ltd., Mumbai. Methyl Orange was purchased from Molychem, Mumbai. All chemicals used were of analytical grade and used as received. All the required solutions were prepared in Millipore water obtained from Millipore Water System (Millipore Corp. Bangalore, India).

2.2 Synthesis of microwave assisted N-TiO₂ nanoparticles

Titanium tetra-isopropoxide (TTIP) 98 % was used as a titanium precursor. N-TiO₂ powder was prepared by controlled addition of 0.1 M TTIP in 100 mL of absolute ethanol with constant stirring to obtain clear solution. Then sufficient amount of surfactant solution (1 % each CTAB and SDS) was added whilst stirring followed by dropwise addition of aqueous ammonia at room temperature until the solution reached a pH 8. After complete precipitation, the precipitate was washed with water and acetone several times to ensure complete removal of impurities. The precipitated solution was subjected to microwave irradiation for 20 min in a microwave oven (Input 900 W, 250 MHz, LG Make,) with on–off cycle (20 on–40 s off). After the microwave irradiation, the dried precipitate was ground using an agate pestle mortar and calcined at different temperatures for 2 h in a PID controlled muffle furnace. The phase purity and the degree of crystallinity of the N-TiO₂ were monitored by XRD.

2.3 Ag loading on N-doped TiO₂ nanocomposites

The prepared N-doped anatase TiO₂ was then modified with silver nanoparticles (NPs) using a simple impregnation and impregnation–reduction method. In a typical preparation of Ag loaded N-doped TiO₂, synthesized N-TiO₂ powder was added to 20 mL of Millipore water and sonicated for 30 min in order to achieve adequate dispersion of the nanopowder. For synthesis of different Ag loading (Ag-T1 to Ag-T4 represents 0.1, 0.5, 1.0 and 1.5 wt% Ag in N-TiO₂), calculated amount of silver nitrate solution was added to the above mixture and then stirred for 60 min so as to form a solution between Ag⁺ and N-TiO₂. Reduction of silver ions was achieved using freshly prepared ice cold sodium borohydride. The prepared Ag loaded N-doped TiO₂ nanocomposite powder was dried at 120 °C for 1 h to remove water.

2.4 Characterization of Ag loaded N-doped TiO₂ nanocomposites

Powder X-ray diffraction (XRD) patterns of N-TiO₂ and Ag loaded N-doped TiO₂ nanocomposites were obtained using a Panalytical diffractometer with CuK α radiation. The shape and size of nanocomposites were obtained from transmission electron microscopy with model TEM, JEOL 3010 (I. I. T. Chennai). Infrared spectra were taken on KBr pellet using a Perkin–Elmer IR spectrometer (Spectrum BX-II). Energy dispersive spectroscopy was used to scan the elemental composition of nanocomposites (EDS JEOL 6360). For the EDS analysis the fine Ag loaded TiO₂

powder was dispersed in isopropanol and few drops of above solution was added on a glass slide (1 cm²) and allowed to evaporate the alcohol. Diffuse reflectance spectra were obtained using a Varian Cary-5000 UV–Vis. NIR spectrophotometer. X-ray photoelectron spectra were recorded by using an ESCA-3000 (VG Scientific Ltd. England) as Al K α radiation (1486.6 eV) with constant pass energy of 50 eV.

2.5 Photocatalytic activity of Ag loaded N-doped TiO₂ nanocomposites

The photocatalytic activity of Ag loaded N-doped TiO₂ nanocomposites were evaluated by monitoring the degradation of MO by using both UV light (365 nm) and sunlight. To evaluate the optimum photocatalytic activity of nanocomposites, the amount was varied from 0.5 to 2 g/dm³ in MO solution (20 ppm). The photoreactor was kept open in air to get sufficient amount of oxygen for photo-oxidation reaction. Typically in this experiment photocatalyst was added in photoreactor containing 100 mL of MO. Before irradiation of light, the solution was stirred for 30 min in dark to ensure adsorption–desorption equilibrium, then exposed to full sunlight at ambient temperature. At particular time intervals aliquots were withdrawn from the photoreactor and the nanoparticles were separate from solution by centrifugation process. The clear dye solution was used to monitor the concentration of MO by recording the absorbance using UV–Vis. double beam spectrophotometer (Shimadzu, Model-UV-3600).

3 Results and discussion

3.1 XRD

The XRD study was done to confirm the phase purity and crystallinity of the nanocomposites. The crystallinity is imperfect if calcination temperature is too low, the well defined crystalline material was formed at 250 °C and this temperature was chosen as a calcination temperature throughout the work [21]. The XRD pattern of N-TiO₂ with anatase phase as shown in Fig. 1. For the different Ag wt% loading, the diffraction pattern reveals that pure anatase N-TiO₂ is formed having diffraction peaks at 25.25°, 37.84°, 47.84°, 53.94°, 55.00°, 62.8°, 68.7°, 70.2°, 75.34°, 82.69° and indexed to the crystal planes of [101], [004], [200], [105], [211], [204], [116], [220], [215], [303]. 2 θ value corresponding to [101] main peak for anatase N-TiO₂ according to JCPDS 01-084-1286 is 25.325 which shifted to lower value 25.258 this may be due to doping of nitrogen in TiO₂ [28]. Major peak for N-TiO₂ was found to be almost same for Ag loaded N-doped TiO₂ nanocomposites except the changes in intensity of peaks. The appearance of

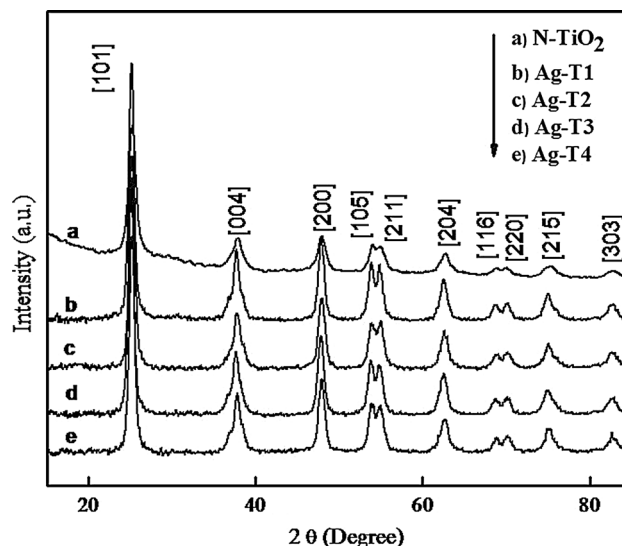


Fig. 1 XRD patterns of N-TiO₂ Ag nanocomposites with different compositions. *a* N-TiO₂, *b* Ag-T1 (0.1 wt%), *c* Ag-T2 (0.5 wt%), *d* Ag-T3 (1.0 wt%) and *e* Ag-T4 (1.5 wt%)

Ag peaks was not observed in the XRD pattern, this may be due to low content of Ag and also high dispersion of Ag nanoparticles on the surface of N-TiO₂. As the Ag loading content increased from 0.0 to 0.5 wt% broadening of diffraction peaks gradually increases that may be due to small crystallite size of nanocomposites. The average crystallite size was calculated by Scherrer's equation [29].

$$\tau = \frac{(0.9\lambda)}{(\beta \cos\theta)} \quad (1)$$

where λ is the X-ray wavelength in Å, β is the full width at half maximum (FWHM) in radians. The pure anatase N-TiO₂ crystallite size was found to be 10 nm and decrease to 8 nm for 0.5 wt% Ag, thereafter the crystallite size was more or less constant.

3.2 XPS analysis of N-TiO₂ Ag nanocomposites

The survey spectrum of Ag loaded N-doped TiO₂ nanocomposites is shown in Fig. 2a of the Ti, O, N, C and Ag elements. The C 1s peak located at 283.9 eV was due to organic remnant of precursor. The values of binding energy for Ti 2p_{3/2} and Ti 2p_{1/2} of pure TiO₂ have been reported as 459.3 and 465.0 eV respectively [30]. The binding energy for Ti 2p_{3/2} and Ti 2p_{1/2} in case of N doped TiO₂ decreases to 458.14 and 463.93 eV respectively as shown in Fig. 2b. This suggests that oxygen in the TiO₂ lattice is partly substituted by nitrogen. Further loading of Ag on N-TiO₂ decreases the binding energy to 458.09 and 463.5 eV respectively. Shifting of the Ti peaks towards the lower binding energy indicates the successful loading of Ag and N [26]. The O 1s XPS spectra shows the peak for Ag

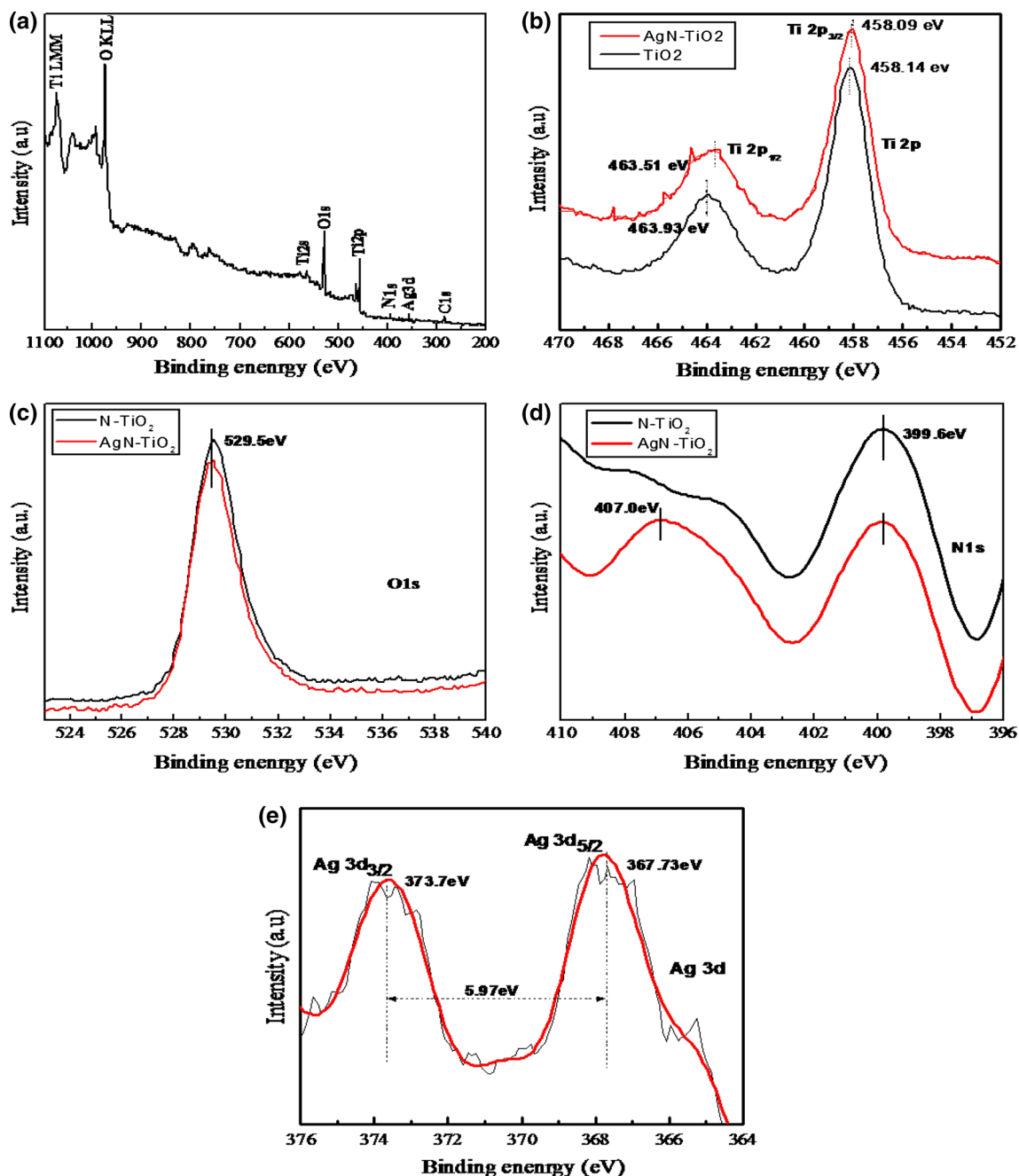


Fig. 2 X-ray photoelectron spectroscopy spectra of N-TiO₂ Ag nanocomposites. **a** The survey spectrum of N-TiO₂, **b** Ti 2p XPS core spectra, **c** O 1s XPS core spectra, and **d** N 1s XPS core spectra, **e** Ag 3d XPS core spectra

loaded N-doped TiO₂ nanocomposite and N-TiO₂ at 529.93 eV as shown in Fig. 2c which is consistent with that of oxygen when N doped in TiO₂ lattice [31]. For the Ag loaded N-doped TiO₂ nanocomposite a peak at 407.0 eV was observed which is not detected in N-TiO₂ as shown in Fig. 2d, suggesting that nitrogen is bonded to oxygen as nitrates [32]. The N 1s XPS peak with a core level binding energy of 399.6 eV is observed in both N-TiO₂ and Ag loaded N-doped TiO₂ which is shown in Fig. 2d this may be due to O–Ti–N structure where some O atoms were

substituted. Similar results were also reported by Cheng et al. [33]. In Fig. 2e the difference of 5.97 eV between peak of Ag 3d_{5/2} and 3d_{3/2} located at 367.73 and 373.7 eV indicates the presence of metallic silver [34].

3.3 Diffuse reflectance spectra of Ag loaded N-doped TiO₂ nanocomposites

The UV–Vis diffuse reflectance spectra of N-doped TiO₂ and Ag loaded N-doped TiO₂ nanocomposites calcined at 250 °C

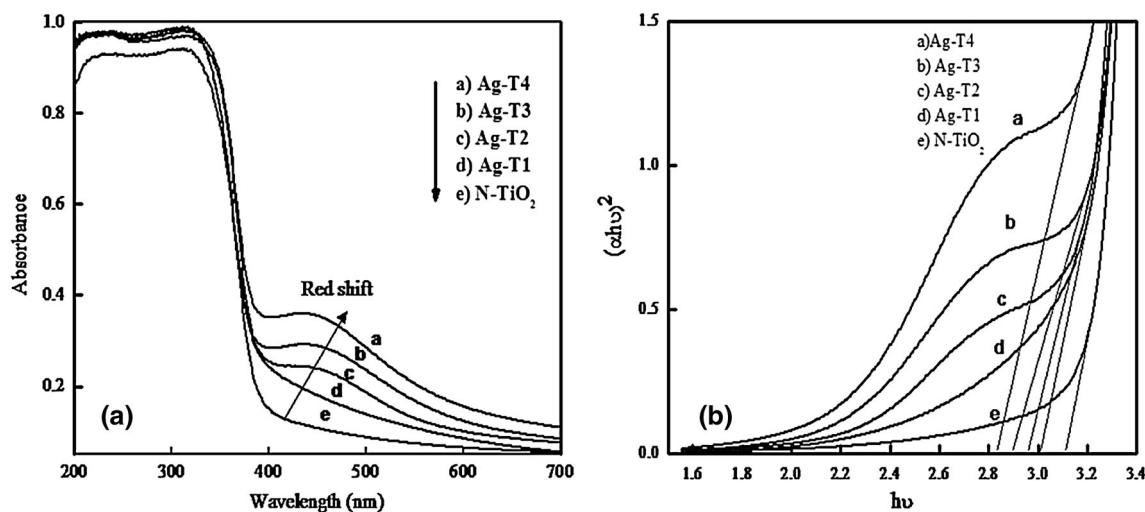


Fig. 3 **a** DR-UV spectra and **b** Tauc plot of N-TiO₂ and N-TiO₂ Ag nanocomposites. *a* Ag-T4 (1.5 wt%), *b* Ag-T3 (1.0 wt%), *c* Ag-T2 (0.5 wt%), *d* Ag-T1 (0.1 wt%), *e* N-TiO₂

are shown in Fig. 3A. It is seen from the spectra that absorption edges are shifted to the visible region due to insertion of nitrogen. The shifting towards visible region and hump was possibly surface plasmon of Ag nanoparticles [35]. The band gap energy is important for normal photocatalytic applications because the energy of incident light must be greater than or equal to the band gap energy. Therefore, the relationship between the absorption coefficient and the photon energy were obtained from Tauc equation.

$$(\alpha hv) = A(hv - E_g)^n \tag{2}$$

where α , v , A , and E_g are the absorption coefficient, frequency, proportionality constant and band gap energy respectively. In the above equation ‘ n ’ dictates the type of transition of semiconductor; in TiO₂ the type of transition is direct type [36] so $n = 0.5$. The band gap of N-TiO₂ decreases from 3.10 to 2.81 eV as Ag content increases from 0.0 to 1.5 wt% (as shown in Fig. 3B).

3.4 Photoluminescence spectra of Ag loaded N-doped TiO₂ nanocomposites

The photoluminescence phenomena are associated with electron–hole pair recombination. Therefore photoluminescence (PL) studies of Ag loaded N-TiO₂ has been undertaken. It is well known fact that the PL emission results from the recombination of electron and hole pairs hence lower the intensity of PL denotes low rate of recombination [37]. Figure 4 shows the PL spectra of Ag loaded N-doped TiO₂ nanocomposites, where the PL intensity of the 0.5 wt% Ag sample is significantly lower than that of the 1.5 wt% Ag indicating that recombination of charge carriers are effectively suppressed. At higher loading of Ag it acts as electron recombination centre, this leads to increase of PL intensity due to fast recombination electron and

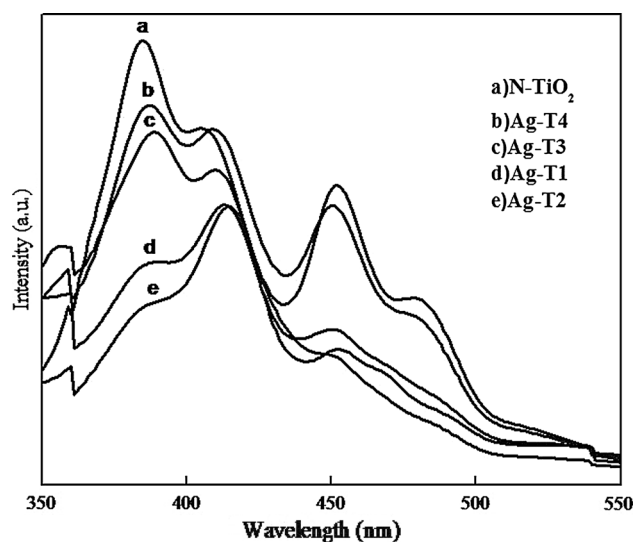


Fig. 4 Photoluminescence spectra of N-TiO₂ and N-TiO₂ Ag nanocomposites. *a* N-TiO₂, *b* Ag-T4 (1.5 wt%), *c* Ag-T3 (1.0 wt%), *d* Ag-T1 (0.1 wt%), *e* Ag-T2 (0.5 wt%)

hole pairs [38]. In the present investigation, the highest photodegradation efficiency of photocatalyst is due to lower electron–hole pair recombination which is supported by PL studies. This indicate that low rate of recombination of electron and hole pairs occurred at optimal 0.5 wt% of Ag loaded N-doped TiO₂ nanocomposites.

3.5 FT-IR spectra of N-TiO₂ and Ag loaded N-doped TiO₂ nanocomposites

Figure 5 shows FT-IR spectra of N-TiO₂ and Ag loaded nanocomposites. The spectrum (a) shows the band at

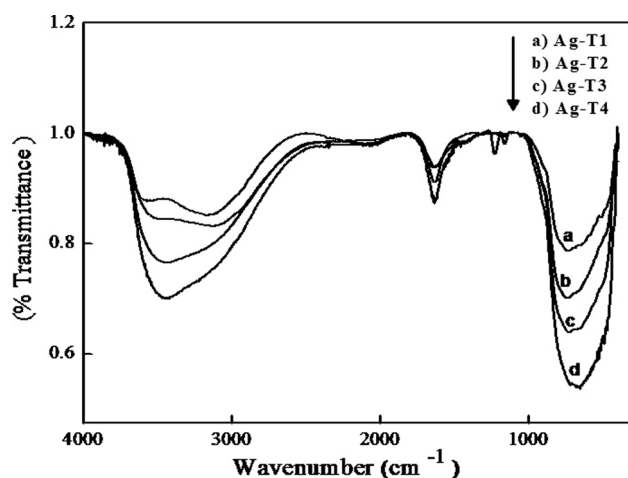


Fig. 5 FT-IR spectra of *a* Ag-T1 (0.1 wt%), *b* Ag-T2 (0.5 wt%), *c* Ag-T3 (1.0 wt%), *d* Ag-T4 (1.5 wt%)

3,471–3,200 cm^{-1} , which is attributed to OH stretching and the band at 1,644 cm^{-1} is due to OH bending of H_2O adsorbed on the surface of the TiO_2 which may have crucial role in the photocatalytic activity of catalyst. The peaks in the range of 2,923–2,825 cm^{-1} correspond to the stretching vibration of C–H bonds which are generated from surfactants. The broad peak at 735–670 cm^{-1} is characteristic of Ti–O bending mode of vibrations which confirms the formation of metal oxygen bonding [39]. The intensity of peak 3,471, 1,644 and 735 cm^{-1} shifted towards lower value after Ag loading [40] indicating the formation of Ag loaded N-doped TiO_2 nanocomposites.

3.6 EDS spectra of Ag loaded N-doped TiO_2 nanocomposites

The elemental composition of synthesized Ag loaded N-doped TiO_2 nanocomposites shown in Fig. 6. The EDS confirmed the presence of Ti, O, N and Ag in synthesized materials as well as revealing the presence of Ag loading. EDS mapping indicates that almost all samples formed were of non-stoichiometry with oxygen deficiency which leads to better performance of photocatalyst [35].

3.7 TEM of Ag loaded N-doped TiO_2 nanocomposites

TEM images of different Ag loaded N-doped TiO_2 nanocomposites are shown in Fig. 7. The size of the particles is in the range 10–15 nm, with the average particle size from representative TEM images to be around 10 nm which is in good agreement with the results obtained from XRD. As the Ag loading increased from 0.1 to 0.5 wt%, the particle size of synthesized nanomaterials were decreased [27] and with further increase in Ag loading the particle size

increased most likely as a result of agglomeration as seen in the TEM images. Lattice fringes can be clearly seen in HRTEM which is shown in Fig. 8a indicating that the d spacing for Ag [111] and TiO_2 [101] planes are 0.24 and 0.35 nm respectively which is in good agreement with results obtained from XRD. SAED patterns for Ag loaded N-doped TiO_2 nanocomposites are shown in Fig. 8b.

3.8 Factors affecting on photocatalytic degradation of methyl orange

3.8.1 Effect of preparation methods

The photocatalysis results demonstrated that impregnation–reduction is superior as compared to the impregnation method on the degradation of MO. The shifting of wavelength (λ_{max}) of dye with uneven changes in intensity was obtained for MO degradation under UV light as shown in Fig. 9A. This may be due to leaching of Ag nanoparticles from catalyst that can be interacted with MO [41]. The result obtained from the impregnation–reduction method do not shown any uneven changes in absorption spectra of MO which is shown in Fig. 9B.

3.8.2 Effect of irradiation sources

Figure 10a shows the absorption spectra of MO during the course of the photochemical reaction under sunlight, at 30 min the band intensity at 464 nm begins to decrease but band intensity at 270 nm increase up to 30 min., may be due to the aromatic rings in MO started to degrade forming a mono substituted ring as a result intensity at 270 nm increases [42]. After 60 min, intensity at 270 nm tends to decrease. At 90 min both the peaks at 270 and 464 nm were disappeared, this indicates that the MO converted into CO_2 and H_2O . Also Fig. 10b shows the absorption spectra of MO under UV. It is observed that there is no shift in the wavelength of MO during the course of photochemical reaction.

Photocatalytic results showed that a 99.6 and 88.76 % degradation of MO were achieved when it was irradiated under UV and sunlight respectively within 90 min. Girginov et al. [43] reported on the photocatalytic activity of Ag doped TiO_2 nanoparticles; the optimal doping content of Ag; MO was degraded up to 65 and 87 % by using UV light and sunlight within 5 h and 120 min. respectively. The results obtained in our case are far better than that reported by Girginov et al. Initially degradation efficiency of MO increases very fast under UV as compared to sunlight; similar results were also reported by Neppolian et al. [44]. To date there are number of reports on degradation of dye by using UV light which is not only hazardous but also expensive because of large input of electrical power

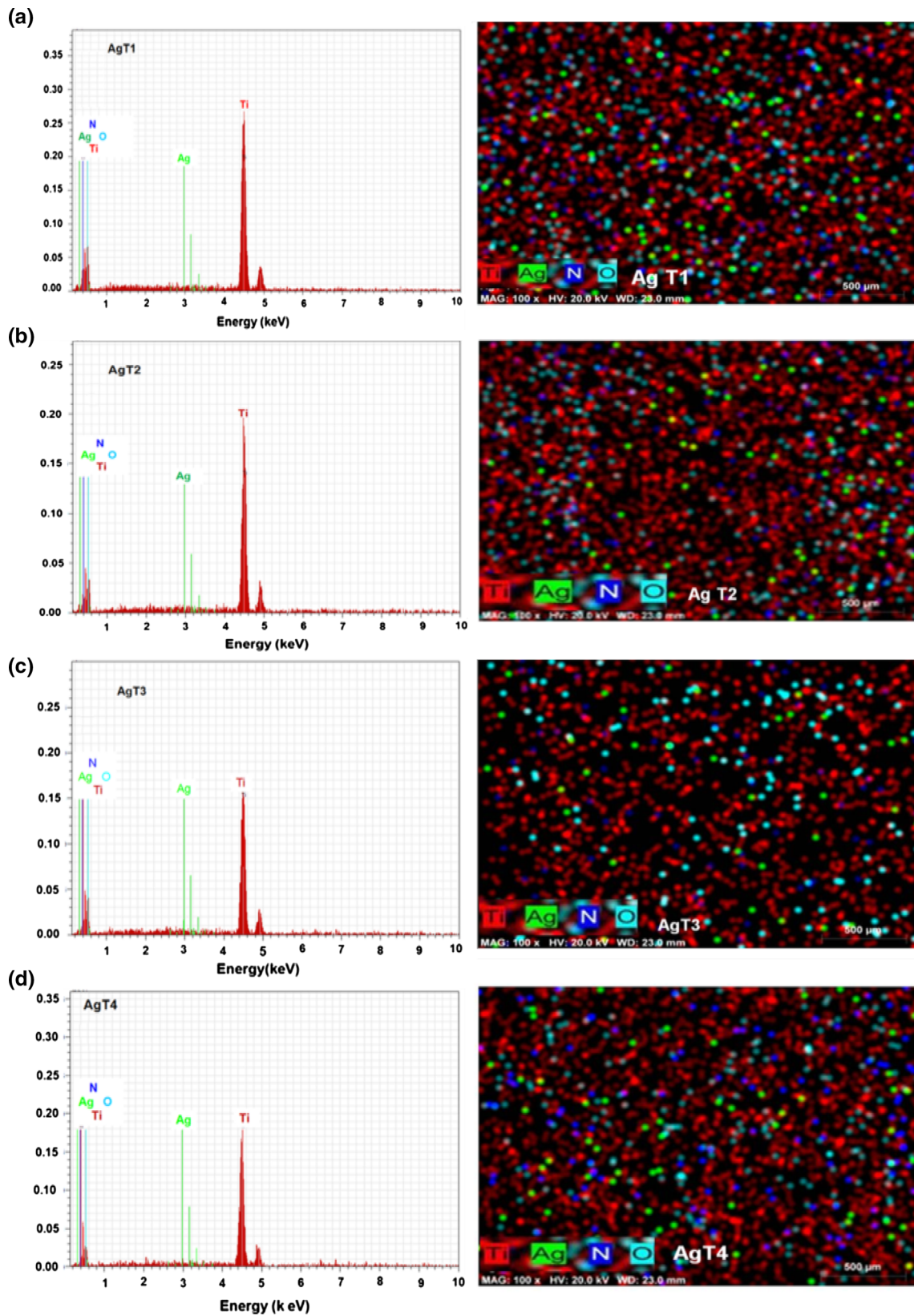


Fig. 6 EDS and its mapping of **a** Ag-T1 (0.1 wt%), **b** Ag-T2 (0.5 wt%), **c** Ag-T3 (1.0 wt%), **d** Ag-T4 (1.5 wt%)

Fig. 7 TEM images of **a** Ag-T1 (0.1 wt%), **b** Ag-T2 (0.5 wt%), **c** Ag-T3 (1.0 wt%), **d** Ag-T4 (1.5 wt%)

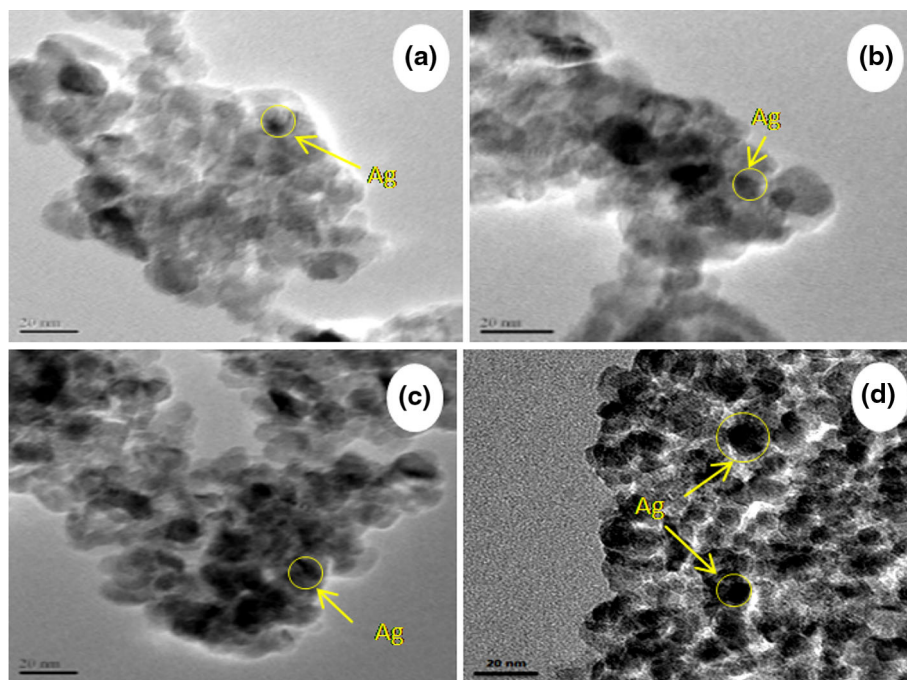
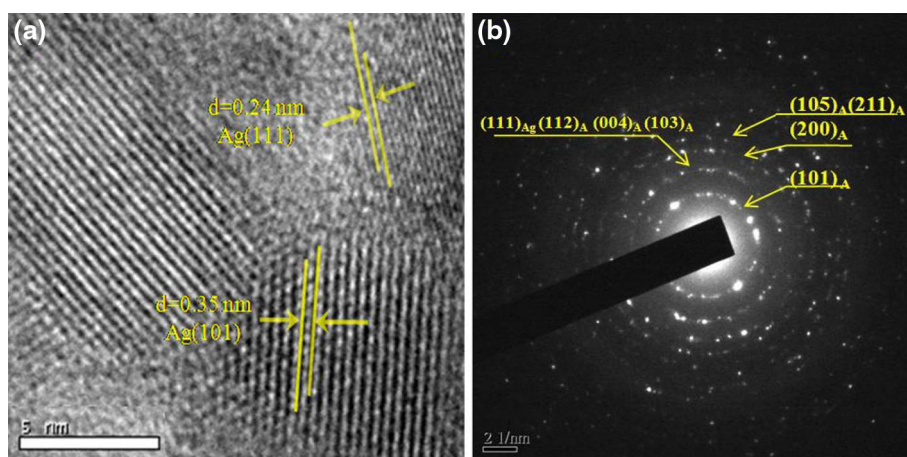


Fig. 8 **a** HRTEM (with lattice fringes) and **b** SAED pattern N-TiO₂ Ag nanocomposites



whereas sunlight is free, safe, and abundant. To overcome the effects of UV light such as DNA damage, skin cancer, acute chronic health effect and to reduce the cost of UV light. Therefore, sunlight was used as the light source for further photocatalytic examinations.

3.8.3 Effect of catalyst loading

The effect of catalyst loading on photocatalytic degradation of MO under sunlight was studied using various amount of catalyst, from 0.5 to 2.0 g/dm³ by keeping other parameters identical. The effect of catalyst loading on photocatalytic degradation of MO is shown in Fig. 11a. A maximum 94.51 % degradation of MO was obtained at 1.0 g/dm³ catalyst loading under sunlight within 120 min. According to

Langmuir–Hinshelwood kinetics model, experimental values fitted into kinetic equation $\ln(C_0/C) = kt$ where k is rate constant, C_0 and C are the initial and concentration at time t respectively. Figure 11b shows the plot of $\ln(C_0/C)$ versus time t , the photocatalytic reaction shows the linear relationship with regression coefficient close to one indicating the photodegradation of MO follows pseudo-first order at low concentration of substrate. Initially as the amount of catalyst increases from 0.5 to 2 g/dm³ rate constant gradually increases from 5.26×10^{-3} to $20.4 \times 10^{-3} \text{ min}^{-1}$ and then decreases to $5.38 \times 10^{-3} \text{ min}^{-1}$. The maximum rate constant was found to be at 1.0 g/dm³ which may be due to the large number of active sites for the adsorption of the dyes and the number of photon absorbed by catalyst. It was found that large amount of catalyst may resulted into the agglomeration

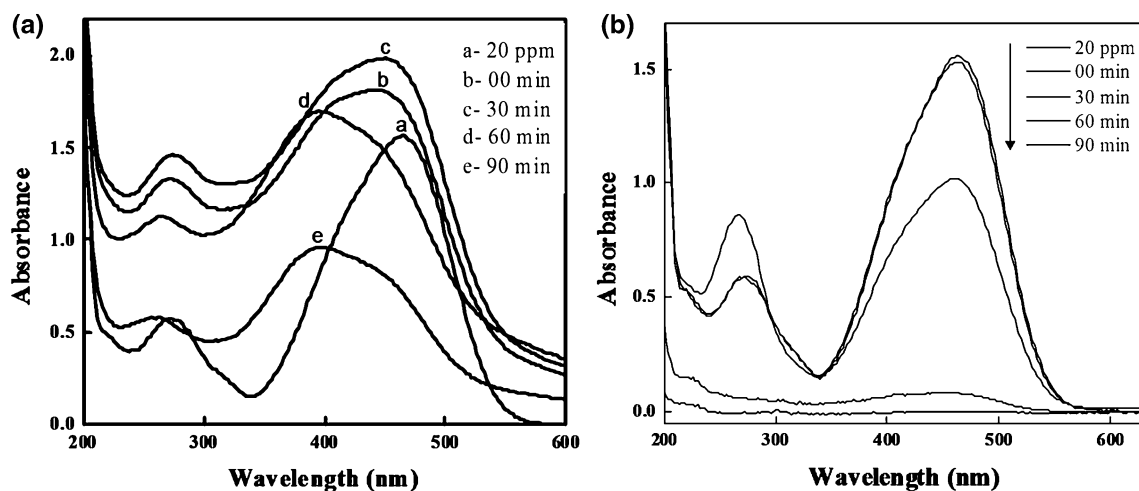


Fig. 9 Degradation of methyl orange under UV light by using catalyst prepared by a impregnation, b impregnation–reduction method

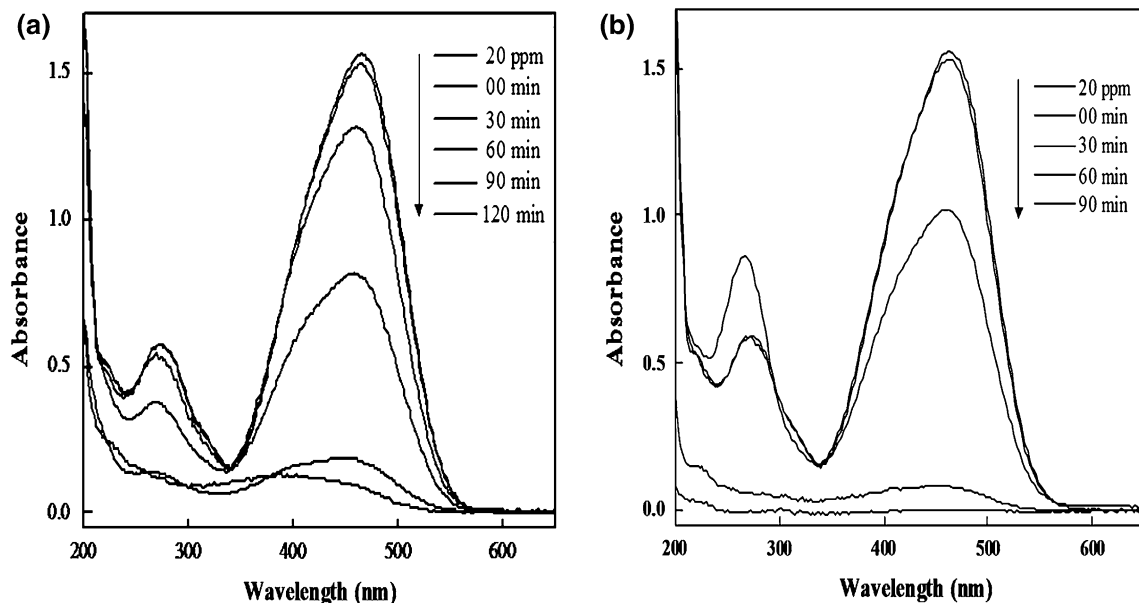


Fig. 10 Methyl orange degradation under a sunlight, b UV light

of catalyst due to this active sites on the catalyst surface becomes unavailable for photon absorption. Another reason for the decreased degradation is turbidity of suspension [45], which causes scattering effect [46]. This is attributed to the inhibition of photon absorption by surface of Ag loaded N-doped TiO₂ nanocomposites.

3.9 Photocatalytic activity of Ag loaded N-doped TiO₂ nanocomposites

The Ag loaded N-doped TiO₂ nanocomposites consist of different routes of photocatalytic activities under UV and sunlight as illustrated in Fig. 12 and described below:

3.9.1 Pathway A

The band gap of Ag loaded N-doped TiO₂ nanocomposite was effectively narrowed by mixing of N 2p orbital and O 2p orbital. Photo excited electrons get transferred from TiO₂ to Ag NPs due to lower Fermi level of silver ($E_f = 0.4$ V). This increases the accumulation of electrons and hence shifting of the Fermi level of composite closer to the conduction band of TiO₂ resulting in an increase in reduction power of the photocatalyst. Therefore the improved charge separation and increased reductive power would be responsible for photocatalytic activity in UV light [47].

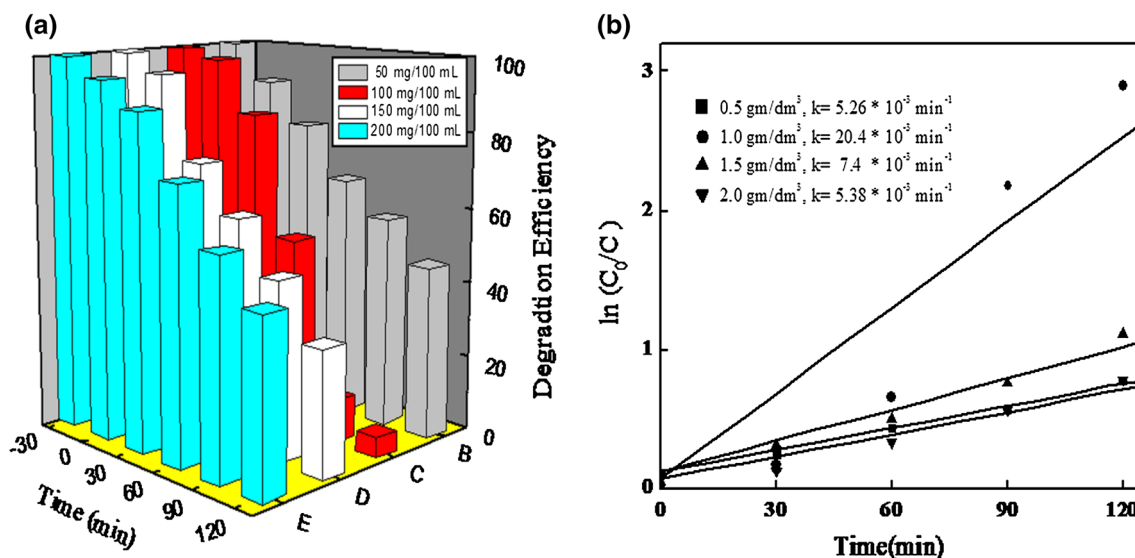


Fig. 11 Catalyst loading of N-TiO₂ Ag nanocomposites. **a** 3d graph methyl orange degradation. **b** $\ln(C_0/C)$ versus time

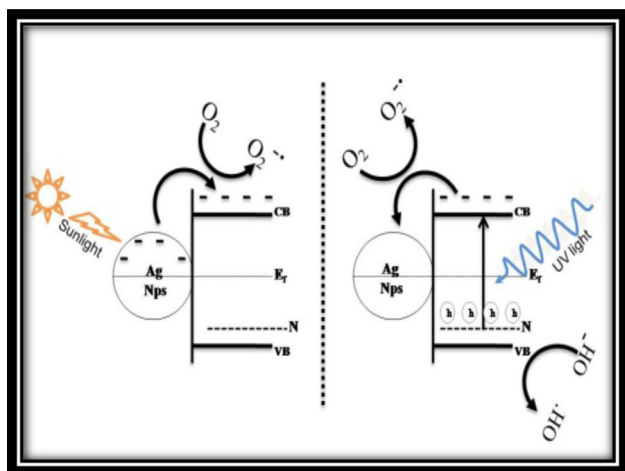


Fig. 12 Probable degradation mechanism in sunlight and UV light

3.9.2 Pathway B

Photocatalytic activity of Ag loaded N-doped TiO₂ nanocomposites in the presence of sunlight is a composite effect of both N-doping and surface plasmon resonance of Ag nanoparticles. The doping with nitrogen decreases the band gap of TiO₂. Along with N-doping, SPR of Ag nanoparticles will help to absorb the light in the visible region. An excited electrons in Ag nanoparticles gets transferred to conduction band of TiO₂, further these electrons were used to generate free radicals which enhances the photocatalytic activity. Moreover, with the increased Ag content the size of Ag NPs becomes bigger and the process of hole capturing by Ag NPs also increases that leads to decrease in photocatalytic activity [48].

4 Conclusions

In this work, the synthesis of N-TiO₂ in pure anatase form by using simple, rapid, energy efficient, ecofriendly and cost effective microwave assisted technique is reported. Further, the modifications of N-TiO₂ by Ag nanoparticles were done by using impregnation–reduction method in order to arrest the rate of recombination of electron hole pairs. The diffuse reflectance spectra showed an absorption edge shifted from 375 to 420 nm along with a small hump due to SPR of Ag. The EDS spectra, mapping and XPS spectra supports presence of nitrogen and silver in TiO₂. In all nanocomposites the deficiency of oxygen was observed that results into better photocatalytic activity. The kinetic study of MO degradation showed pseudo first order kinetics. The highest rate constant ($2.04 \times 10^{-2} \text{ min}^{-1}$) was observed at 1.0 g/dm³ catalyst. From the photodegradation experiments it was found that 94.51 % degradation of MO was achieved within 2 h when N-TiO₂ Ag nanocomposites was used under sunlight. An enhancement in efficiency of about 40 % was achieved successfully by Ag loading as compared to N-TiO₂.

Acknowledgments One of the authors (KMG) is thankful to DST, New Delhi, India for providing the Financial Support under Major Research Project: SR/S1/PC/0041/2010. Authors are also thankful to Director, SAIF, NEHU, Shilong for providing TEM facility.

References

1. H. Sun, Y. Bai, Y. Cheng, W. Jin, N. Xu, Ind. Eng. Chem. Res. **45**, 4971–4976 (2006)
2. S. Tojo, T. Tachikawa, M. Fujitsuka, T. Majima, J. Phys. Chem. C **112**, 14948–14954 (2008)

3. M.S. Wong, S.W. Hsu, K.K. Rao, C.P. Kumar, *J. Mol. Catal. A: Chem.* **279**, 20–26 (2008)
4. P.P. Hnakare, R.P. Patil, A.V. Jadhav, K.M. Garadkar, R. Sasikala, *Appl. Cat. B: Environ.* **107**, 333–339 (2011)
5. H. Kato, A. Kudo, *J. Phys. Chem. B* **106**, 5029–5034 (2006)
6. A. Fujishima, K. Honda, *Nature* **238**, 37–38 (1972)
7. C.C. Chen, C.S. Lu, Y.C. Chung, J.L. Jan, *J. Hazard. Mater.* **141**, 520–528 (2007)
8. Q. Sun, Y. Xu, *J. Phys. Chem. C* **114**, 18911–18918 (2010)
9. C. Tiejun, L. Yuchao, P. Zhenshan, L. Yunfei, W. Zongyuan, D. Qian, *J. Environ. Sci.* **21**, 997–1004 (2009)
10. X. Chenga, X. Yua, Z. Xing, *Appl. Surf. Sci.* **258**, 7644–7650 (2012)
11. R. Su, R. Tiruvalam, Q. He, N. Dimitratos, L. Kesavan, C. Hammond, J. Antonio Lopez-Sanchez, R. Bechstein, C.J. Kiely, G.J. Hutchings, F. Besenbacher, *ACS Nano* **6**, 6284–6292 (2012)
12. J. Choi, H. Park, M.R. Hoffmann, *J. Phys. Chem. C* **114**, 783–792 (2010)
13. H. Li, Z. Bian, J. Zhu, Y. Huo, H. Li, Y. Lu, *J. Am. Chem. Soc.* **129**, 4538–4539 (2007)
14. Y. Gai, J. Li, S.S. Li, J.B. Xia, S.H. Wei, *Phys. Rev. Lett.* **102**, 36402–36405 (2009)
15. D. Wang, Z.H. Zhou, H. Yang, K.B. Shen, Y. Huang, S. Shen, *J. Mater. Chem.* **22**, 16306–16311 (2012)
16. P. Zhang, C. Shao, Z. Zhang, M. Zhang, J. Mu, Z. Guo, Y. Sun, Y. Liu, *J. Mater. Chem.* **21**, 17746–17753 (2011)
17. H. Zhang, G. Chen, *Environ. Sci. Technol.* **43**, 2905–2910 (2009)
18. M.L. de Souza, P. Corio, *Appl. Cata. B: Environ.* **136**, 325–333 (2013)
19. E. Kowalska, O. Omar Prieto Mahaney, R. Abe, B. Ohtani, *Phys. Chem. Chem. Phys.* **12**, 2344–2355 (2010)
20. S. Sarina, B. Sagala, Y. Huang, C. Chen, E. Jaatinen, J. Jia, G.A. Ayoko, B. Zhaorigetu, H. Zhu, *Green Chem.* **16**, 331–341 (2014)
21. B. Xin, L. Jing, Z. Ren, B. Wang, H. Fu, *J. Phys. Chem. B* **109**, 2805–2809 (2005)
22. T.C. Damato, C.C.S. de Oliveira, R.A. Ando, P.H.C. Camargo, *Langmuir* **29**, 1642–1649 (2013)
23. J.T. Park, J.H. Koh, J.A. Seo, Y.S. Cho, J.H. Kim, *Appl. Surf. Sci.* **257**, 8301–8306 (2011)
24. V.K. Sharma, R.A. Yngard, Y. Lin, *Adv. Colloid Interface Sci.* **145**, 83–96 (2009)
25. E. Stratakis, E. Kymakis, *Mater. Today* **16**, 133–146 (2013)
26. Y. Gao, P. Fang, F. Chen, Y. Liu, Z. Liu, D. Wang, Y. Dai, *Appl. Surf. Sci.* **265**, 796–801 (2013)
27. M. Wu, B. Yang, Y. Lv, Z. Fu, J. Xu, T. Guo, Y. Zhao, *Appl. Surf. Sci.* **256**, 7125–7130 (2010)
28. K.M. Reddy, S.V. Manorama, A.R. Reddy, *Mater. Chem. Phys.* **78**, 239–245 (2002)
29. K.M. Garadkar, L.A. Ghule, K.B. Sapnar, S.D. Dhole, *Mater. Res. Bull.* **48**, 1105–1109 (2013)
30. X. Chen, C. Burda, *J. Phys. Chem. B* **108**, 15446–15449 (2004)
31. J. Wang, D.N. Tafen, J.P. Lewis, Z. Hong, A. Manivannan, M. Zhi, M. Li, N. Wu, *J. Am. Chem. Soc.* **131**, 12290–12297 (2009)
32. S. Sakthivel, M. Janczarek, H. Kisch, *J. Phys. Chem. B* **108**, 19384–19387 (2004)
33. X. Cheng, Z. Xing, X. Yu, *Appl. Surf. Sci.* **258**, 3244–3248 (2012)
34. L. Gomathi Devi, K.M. Reddy, *Appl. Surf. Sci.* **257**, 6821–6828 (2011)
35. K.M. Fujimaki, C. Rockstuhl, J. Tominaga, H. Murakami, Y. Ohki, N. Yoshida, T. Watanabe, *J. Am. Chem. Soc.* **130**, 1676–1680 (2008)
36. G. Sauthier, E. György, A. Figueras, R.S. Sanchez, J. Herno, *J. Phys. Chem. C* **116**, 14534–14540 (2012)
37. Y. Yang, J. Wen, J. Wei, R. Xiong, J. Shi, C. Pan, *ACS Appl. Mater. Interfaces* **5**, 6201–6207 (2013)
38. X. Pan, Y.-J. Xu, *J. Phys. Chem. C* **117**, 17996–18005 (2013)
39. T. Uddin, Y. Nicolas, C. Olivier, T. Toupance, M.M. Müller, H.J. Kleebe, K. Rachut, J. Ziegler, A. Klein, W. Jaegermann, *J. Phys. Chem. C* **117**, 22098–22110 (2013)
40. G. Liu, H.G. Yang, X. Wang, L. Cheng, H. Lu, L. Wang, G.Q. Lu, H.M. Cheng, *J. Phys. Chem. C* **113**, 21784–21788 (2009)
41. W.Y. Hui, S.J. Hong, *Acta Phys. Chim. Sin.* **28**, 1313–1319 (2012)
42. S. Qaradawi, S.R. Salman, *J. Photochem. Photobiol. A: Chem.* **148**, 161–168 (2002)
43. C. Girginov, P. Stefchev, P. Vitanov, Hr Dikov, *J. Eng. Sci. Technol. Rev* **5**(4), 14–17 (2012)
44. B. Neppolian, H.C. Choi, S. Sakthivel, B. Arabindoo, V. Murugesan, *J. Hazard. Mater.* **89**, 303–317 (2002)
45. O.K. Mahadwad, P.A. Parikh, R.V. Jasra, C. Patil, *Bull. Mater. Sci.* **34**, 551–556 (2011)
46. S.K. Pardeshi, A.B. Patil, *Sol. Energy* **82**, 700–705 (2008)
47. D. Kong, J.Z. Yie Tan, F. Yang, J. Zeng, X. Zhang, *Appl. Surf. Sci.* **277**, 105–110 (2013)
48. X. Yin, W. Que, Y. Liao, H. Xie, D. Fei, *Colloids Surf. A: Physicochem. Eng. Asp.* **410**, 153–158 (2012)